Experimental Demonstration of the Stabilizing Effect of Dielectric Coatings on Magnetically Accelerated Imploding Metallic Liners

T. J. Awe, K. J. Peterson, E. P. Yu, R. D. McBride, D. B. Sinars, M. R. Gomez, C. A. Jennings,
M. R. Martin, S. E. Rosenthal, D. G. Schroen, A. B. Sefkow, S. A. Slutz, K. Tomlinson, and
R. A. Vesey

Experimental demonstration of the stabilizing effect of dielectric coatings on magnetically-accelerated imploding metallic liners

T.J. Awe[1,*], K.J. Peterson[1], E.P. Yu[1], R.D. McBride[1], D.B. Sinars[1], M.R. Gomez[1], C.A. Jennings[1], M.R. Martin[1], S.E. Rosenthal[1], D.G. Schroen[2], A.B. Sefkow[1], S.A. Slutz[1], K. Tomlinson[2], and R.A. Vesey[1]

[1]Sandia National Laboratories, P.O. Box 5800, Albuquerque, New Mexico 87185, USA
[2]General Atomics, San Diego, California 92121, USA

Enhanced implosion stability has been experimentally demonstrated for magnetically-accelerated liners that are coated with 70 µm of dielectric. The dielectric tamps liner-mass redistribution from electrothermal instabilities and also buffers coupling of the drive magnetic field to the magneto-Rayleigh-Taylor instability. A dielectric-coated and axially-pre-magnetized beryllium liner was radiographed at a convergence ratio ($CR \equiv R_{in,0}/R_{in}(z,t)$) of 20, which is the highest CR ever directly observed for a strengthless magnetically-driven liner. The inner-wall radius $R_{in}(z,t)$ displayed unprecedented uniformity, varying from 95   130 µm over the 4.0 mm axial height captured by the radiograph.

For magnetically-driven z-pinch implosions, a cylindrical conductor carries an axial current density, j_z, which self-generates an azimuthal magnetic field, B . The resultant "$\mathbf{j} \times \mathbf{B}$ force" is directed radially inward, and increases in strength as the system implodes. Z pinches are energy rich and efficient, and they are used broadly in many areas of active high-energy-density-physics research. Magnetically driven experiments effectively examine various dynamic material properties such as equations of state [1], strength [2], and opacity [3]. They also enable studies of radiation-driven hydrodynamic phenomena [4,5], and inertial confinement fusion (ICF) [6]. Their utility is, however, limited by magnetohydrodynamic (MHD) instabilities which rapidly introduce three-dimensional dynamics that destroy plasma symmetry and confinement. Starting as early as the 1950s, much of Z pinch research has been rooted in understanding and mitigating MHD instabilities [7,8,9].

On the Z accelerator [10,11] at Sandia National Laboratories, imploding liners (cylindrical tubes) are shocklessly compressed to multi-megabar pressures in dynamic materials studies [12] and are used to compress deuterium plasmas to inertial confinement fusion (ICF) relevant temperatures and pressures [13]. In MagLIF (Magnetized Liner Inertial Fusion [6,14,15,16], a magnetized ICF concept), nearly 20 MA is delivered to a cm-scale cylindrical beryllium (Be) liner with ~500-µm-thick walls. As it is magnetically accelerated to ~70 km/s, the liner is susceptible to fluid-like instabilities including the magneto-Rayleigh-Taylor (MRT) instability [17,18]. If MRT amplitudes grow to roughly the wall thickness, large variations in the liner's areal density (ρR) will result in poor plasma confinement and reduced fusion yield. In this Letter, we report novel experimental results that demonstrate the dramatic stabilizing effect of applying dielectric coatings and axial magnetic fields to liners that are then rapidly imploded by a magnetic drive. When using these techniques, the observed implosion uniformity is unprecedented, and represents a substantial advancement for magnetically-driven systems.

Conventionally, MRT growth is reduced by minimizing the initial perturbation from which instabilities grow, thus MagLIF-relevant liners are single-point diamond turned to 10-30 nm RMS initial surface roughness. However, initial experiments showed only a ~2X difference in MRT amplitude from a liner with 10-30 nm initial roughness when compared to one seeded with 50-100 µm perturbations (see Figs. 8 and 9 of [19]); this strongly suggested that initial surface roughness was not the dominant seed. Moreover, the resulting MRT structures have an unexpectedly large degree of azimuthal correlation [20,21]. Recent work [22] is consistent with the idea that an electrothermal instability [23,24,25] (ETI), which forms early in the experiment, seeds an azimuthally-correlated perturbation with greater amplitude than the liner's initial roughness. The striation form (**k** in z-direction) of ETI grows rapidly when the liner transitions from solid to liquid to vapor states due to runaway Ohmic heating associated with the

increase in resistivity with temperature ($\partial\eta/\partial T > 0$ in metals; not true for dielectrics) [7,26,27,28,29,30,31]. Unstable temperature (and pressure) growth eventually drives density perturbations in the liner when the heated outer surface of the metal loses strength and expands.

The fundamental physical processes that contribute to the growth of ETI are elucidated by Eqn. 1 (in the linear approximation), where γ is the linear growth rate, ρ is mass density, p is the pressure, η is electrical resistivity, c_v is specific heat capacity, κ is thermal conductivity, k_z is the axial wavenumber, T is temperature, and T* is a material specific temperature that depends on pressure and density through a simplified equation of state (see [29] for derivation, note that uniform current density is assumed).

$$\gamma = \frac{j^2 \dfrac{\partial \eta}{\partial T} + \dfrac{\rho}{T^*}\left(c_v \dfrac{\partial T}{\partial t} - j^2 \dfrac{\partial \eta}{\partial \rho}\right) - k_z^2 \kappa}{\rho c_v + \dfrac{p}{T^*}} \qquad (1)$$

When carrying intense current, condensed metal is destabilized by the effects of increasing resistivity with temperature, (1st term in Eqn. 1, which often dominates), material heating (2nd term), and increasing resistivity with decreasing density (3rd term, which can grow rapidly for $T>T_{melt}$). Short wavelengths are stabilized by thermal conduction (4th term). In general, while in the condensed metal state, the striation form of ETI (**k** in z-direction) grows rapidly with increasing temperature and decreasing density. As the metal transforms to Spitzer-like plasma (with $\partial\eta/\partial T < 0$), the striation form of ETI is stabilized, but before this occurs ETI can seed significant density perturbations.

Principally, a dielectric tamper reduces the instability growth associated with non-uniform expansion of the liner's outer boundary (when the linear theory may no longer apply). Due to the tamper's inertia, the liner density cannot drop as quickly due to ablation of the metal's surface (3rd term in Eq. 1); the otherwise rapid redistribution of mass from non-uniform Ohmic heating is limited, and the seed amplitude for subsequent MRT growth is reduced. At a thickness of 70 um, the dielectric is calculated to provide sufficient tamping since (according to simulations) its mass is about twice the ablated liner mass when the outer wall begins to implode.

Recent experiments examining dielectric-coated solid aluminum (Al) rods have demonstrated a 10X reduction of cumulative MRT growth [22]. While these results are highly encouraging, rapidly accelerated liners incur higher MRT growth than non-imploding solid rods. Also, the time-dependent current density carried by the dielectric cannot yet be quantified. According to 2D simulations, the current carried by the dielectric determines whether the metal-dielectric interface separates, which impacts implosion stability. Since all of our simulations to date are based on MHD codes, we cannot accurately account for dielectric breakdown, motivating the need for these experiments. While quantifying the current density distribution remains an ongoing experimental challenge, the radiographic data in Figs. 2-4 show definitively that the dielectric implodes along with the metallic liner and thus must carry appreciable current.

In this Letter, we report experimental results that demonstrate the dramatic stabilizing effect of dielectric coatings when applied to rapidly-accelerated magnetically-driven imploding liners. First, Al-liner experiments are discussed. Due to Al's relatively high opacity, the Al-dielectric interface remains obvious in radiographs, allowing straightforward evaluation of the metal's outer surface. Next, Be-liner experiments are discussed. Due to the comparable opacity of Be and Epon, locating the Be-dielectric interface is challenging. However, the low opacity of the Be enables characterization of the instability structure, and diagnosis of the liner's inner wall. Finally, data from a dielectric-coated and axially-pre-magnetized Be liner are presented (axial premagnetization is known to enhance liner stability [32,33]). A

radiograph of a dielectric-coated and pre-magnetized Be liner captured at a convergence ratio ($CR=R_{in}(t=0)/R_{in}(z,t)$) of 20 demonstrates unprecedented symmetry.

For this study, uncoated and coated (70 μm Epon epoxy) Al and Be liners are driven with roughly 20 MA of current in 100 ns (Fig. 1(a-b)) by the Z accelerator. Be liners with initial radii $R_{in,0}$=2.89 mm and $R_{out,0}$=3.47 mm (aspect ratio, $AR=R_{out,0}/(R_{out,0}-R_{in,0})$=6,) are "acceleration matched" to Al liners with $R_{in,0}$=3.082 mm and $R_{out,0}$=3.47 mm (AR=8.94, Fig 1(c)); matching the liner mass and $R_{out,0}$, to first order, ensures matched $R_{out}(t)$ and $B_{,out}(t)$ throughout the implosion. Experimental initial conditions are displayed in Fig. 1(c) and further specified in Table 1.
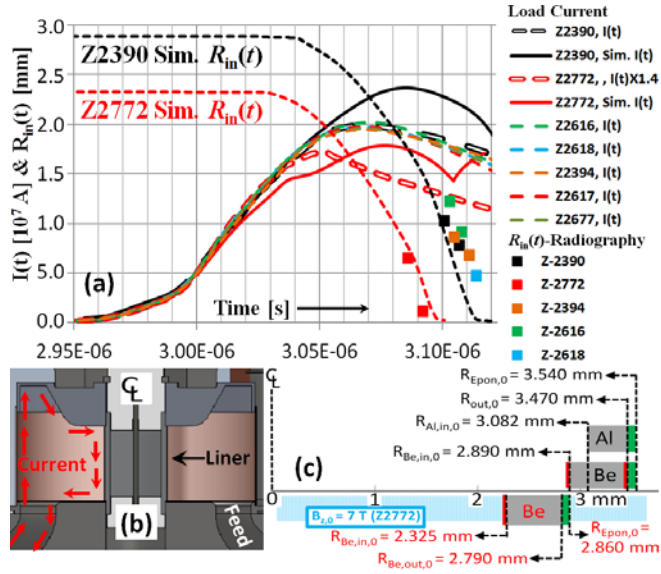

Figure 1: (a) Load current waveforms, $I(t)$, and liner inner-wall trajectories, $R_{in}(t)$. Experimental $I(t)$ data are from Bdot probes located at R~6 cm. All data is time shifted so that $I(t$=3000 ns)=5 MA. Squares indicate axially-averaged $R_{in}(t)$ data from experimental radiographs. Simulated (1D) $I(t)$ and $R_{in}(t)$ curves pertain to Z2390 ($R_{in,0}$=2.89 mm) and Z2772 ($R_{in,0}$=2.325 mm, Z2772 will be discussed in detail later in the paper). For Z2772 (and for all experiments which include axial premagnetization, which require a higher-inductance extended final current feed), Bdot measurements are unphysically low, and load currents are empirically derived. (b) Cross section of typical liner hardware used in Z experiments. (c) Initial geometry of mass-matched Al and Be Epon-coated liners (above horizontal axis) and of a pre-magnetized ($B_{z,0}$=7 T, indicated by blue shading) and coated Be liner (below axis). Epon (shown in green) was cast onto the target surface, and then single-point diamond turned on a lathe to 70 μm thick. Red bars indicate Pt coating locations.

Shot No.	Liner Material	Liner $R_{in,0}$	Liner $R_{out,0}$	$R_{Epon,out,0}$	$B_{z,0}$
2617	Al	3.082	3.47	3.54	0
2677	Al	3.082	3.47	uncoated	0
2390, 2394	Be	2.89	3.47	uncoated	0
2616, 2618	Be	2.89	3.47	3.54	0
2480	Be	2.325	2.79	uncoated	7
2772	Be	2.325	2.79	2.86	7

Table 1. Experimental initial liner geometry and initial axial magnetic field strength.

The differing opacities of Al and Be in 6.151-keV radiographs allow different features of the implosion to be readily observed. (Details of the 2-frame, 1-ns temporal resolution, 15-micron spatial resolution, 6.151-keV monochromatic radiography diagnostic [34] are found in [20,22,32]). For Al with opacity $\kappa_{Al,6.151\ keV}$~100 cm^2/g, radiographs effectively provide liner silhouettes until the outermost Al expands enough to allow transmission through the liner's outer edge. Beryllium's low opacity

($\kappa_{Be,6.151\ keV}$=2.44cm^2/g) allows measurable transmission through the liner's interior. High-opacity platinum (Pt) film is vapor deposited to the Be liner's walls to locally enhance contrast (Fig 1(c)). These thin films were 25 nm thick on the inner surface and 75 nm thick on the outer surface, and they do not significantly alter the implosion hydrodynamics. The Pt tracers are distinct in radiographs only if a degree of cylindrical symmetry can be maintained to provide limb darkening (see [33] for a detailed discussion of the radiographic tracer-layer technique). The use of Pt tracers provided high contrast at the Be liner's inner wall, where 2D or even 1D symmetry was maintained, but it was of little value in identifying the difficult-to-distinguish Be-Epon boundary ($\kappa_{Epon,6.151\ keV}$~10 cm^2/g) where the Pt layer was 3D disrupted and/or radially distributed.

Aluminum-liner experiments demonstrate that a dielectric tamper modifies the liner's edge-density during ablation expansion and reduces cumulative MRT growth by approximately 10X (Fig. 2). For the uncoated liner (Figs. 2(b,d)), large amplitude MRT structure has grown (~300-700 microns, 10% transmission contour). Little mass resides directly outside of "bubble" regions, as can be seen by the local overlap of all transmission contours (Fig. 2(d)). However, large radial-gradient scale lengths exist in the "spike" regions (of order 300 microns from 10% to 60% transmission), where lower-density Al plasma is present. Modulations in the low-density plasma are well correlated with the modulations in the dense metal. By contrast, for the coated liner (Fig. 2(a,c)), the 10%, 15%, and 20% transmission contours are well correlated, but modulations in the higher transmission contours (e.g. the 60% curve) show little-to-no correlation to those in the underlying metal. To quantify the degree of correlation in the transition region from dense metal to low-density plasma, for both the coated and uncoated liners, we use the metric [35],

$$C_{ij} = \int_{L1}^{L2} \Delta r_i(z) \Delta r_j(z) dz \left/ \sqrt{\int_{L1}^{L2} \Delta r_i^2(z) dz \int_{L1}^{L2} \Delta r_j^2(z) dz} \right. \qquad (2)$$

where C_{ij}=1 implies perfect correlation, C_{ij} =0 implies no correlation, and C_{ij} =-1 implies perfect anti-correlation (note that the respective means of the contours under evaluation, $r_i(z)$ and $r_j(z)$, must be subtracted so that each function averages to zero). For the 10% and 60% curves of the uncoated liner (Fig. 2(d)) $C_{10\%,60\%}$=0.82. The high correlation and the low gradient scale length in the bubble regions allows the driving azimuthal magnetic field to readily couple to instabilities near the liner's outer surface. For the coated liner, the Epon-generated plasma is uncorrelated with the underlying metal (Fig 2(c), $C_{10\%,60\%}$=.05), yet fills the perturbations in the dense metal. Therefore, at this advanced stage of the implosion, the instabilities in the coating have not fed through to the liner, and the coating is still providing a tamping effect. Furthermore, since this Epon plasma implodes with the liner at 10's of km/s, it must carry appreciable current and thus support a broadened current distribution, which may ultimately reduce the MRT growth rate [36]. The practical implications of these effects are not fully understood and are currently being evaluated computationally.
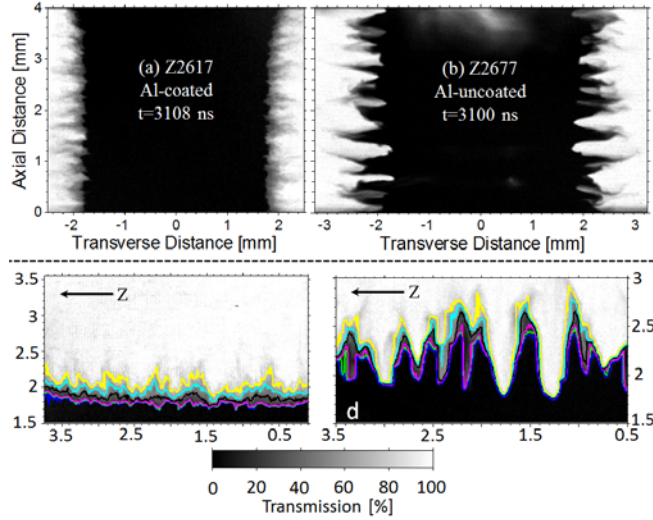
Figure 2. Radiographs of AR=8.94 Al liners ($R_{in,0}$=3.082 mm, and $R_{out,0}$=3.47 mm). (a) Dielectric coated. (b) Uncoated. (c), and (d) Transmission contours of the right-hand side surfaces of the radiographs in (a) and (b), respectively. Transmission contours are (percentage–color): (10%–blue), (15%–green), (20%–magenta), (40%–black), (60%–cyan), and (80%–yellow). Figure (c) extends to the initial radius of the Epon ($R_{Epon,out,0}$=3.54 mm). Transmission is nearly 100% for radii from 2.5 mm to 3.5 mm which demonstrates that the Epon coating has imploded with the liner. The grayscale applies to (a-d).

Beryllium liners retain acceptable contrast in radiographs throughout the implosion, which enables analysis of instabilities and characterization of the liner's inner wall. As indicated by the periodic dark and light bands (**k** in z-direction), the uncoated Be liners in Figs. 3(c-d) display large-amplitude and highly-azimuthally-correlated MRT instabilities. By contrast, for coated liners, radiography reveals low amplitude variations in opacity with almost no discernable azimuthal correlation (compare Figs 3(a) and 3(c), which are at nearly the same convergence). This shows that azimuthally-correlated structure is of low amplitude and/or that the instability structure is predominantly 3D-like. (Note that structures without 1D or 2D symmetry are difficult to identify in penetrating radiography, since the diagnostic provides a measure of the material opacity integrated along an x-ray chord that is normal to the r-z-plane.) Early in the implosion, instability feedthrough is reduced for coated liners (again, compare 3(a) and 3(c), particularly the straightness of the liner's inner wall). Whether or not this increased uniformity persists at higher convergence cannot be determined from this dataset due to an electrode instability, which formed at the anode (top) end of the liner, resulting in the observed axial "zippering" and 6.151-keV x-ray emission in the top half of Fig. 3(b).
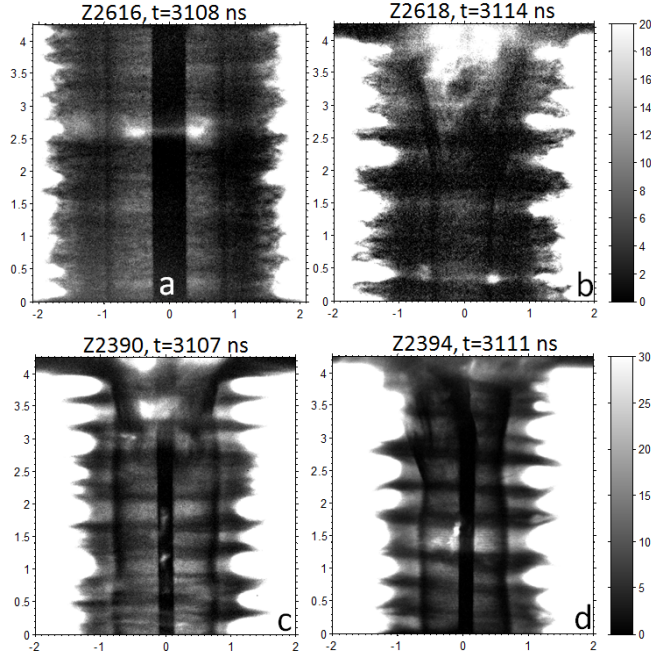
Figure 3. Radiographs of imploding Be liners with AR=6, $R_{in,0}$=2.89 mm, and $R_{out,0}$=3.47 mm. Axes in [mm]. Transmission scales in [%]. (a)-(b) Dielectric coated. (c)-(d) Uncoated liner experiments previously reported in [20]. Rods are placed on axis in select experiments (black vertical strips in the center of radiographs a, c, and d) to limit the time-integrated self-emission that is sometimes generated at stagnation, and can obscure radiographs. To accentuate the high-opacity coatings on the liner's inner wall, the grayscale ranges were limited to 0-30% transmission in (a), (c), and (d) (0%=black, 30%=white), and 0-20% transmission in (b). Therefore, much of the Be and Epon mass in the limb regions of the radiographs has been omitted in this representation of the data.

An experiment designed to evaluate the combined stabilizing effects of a dielectric mass tamper and a pre-imposed axial magnetic field resulted in the most stable material-strength-free magnetically-driven liner implosion ever observed (Figs. 4(a-b)). A dielectric-coated (70 μm thick coating) AR-6 Be liner was pre-magnetized with a 7 T axial magnetic field [37]. The enhanced stability is likely the result of several effects. First, pre-magnetized liners develop helix-like instability structure (Fig 4(c)) with reduced coupling to the B drive field ($\mathbf{k} \cdot B_\theta \neq 0$). Second, the inclusion of the dielectric tamper results in a finer-scale helical instability structure. The helical modes in Fig. 4(b) appear to be either decoupled from or to have not yet fed through to the liner's inner wall.
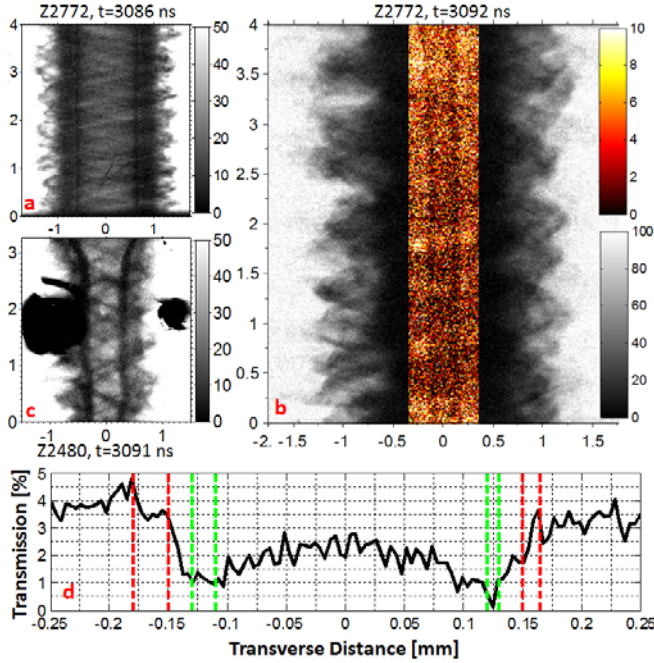
Figure 4. (a) and (b) Radiographs of a dielectric coated and pre-magnetized AR-6 Be liner. In (b), data from a single radiograph is displayed using two transmission scales. For R<300 μm, the transmission range is limited to 0-10% to accentuate the liner's inner wall. For R>300 μm, the transmission range is 0-100% allowing observation of the full liner mass. The liner in (c, data previously reported in [32]), was similar to the liner in (a) and (b), including the 7-T axial premagnetization field, but did not include a dielectric coating. Remarkably, even at CR=6.4, the liner in (c) has larger amplitude inner-wall instabilities than the liner in (b), which is at CR~20. The liner in (a-b) contained a 60 psi deuterium gas fill, whereas the liner in (c) contained s 120 psi deuterium fill; simulations suggest that inclusion of cold gas does not play a meaningful role in the dynamics of these liners, as the back pressure (even at high convergence) is insignificant. (d) Transmission profile of the central region of the radiograph in (b), axially averaged from z=2.0 mm to z=2.67 mm. (a-c) Axes in [mm]. Transmission scales in [%].

The inner wall of the liner in Fig. 4(b) has been characterized by analyzing radial transmission profiles to locate the reduction in transmission associated with the 25-nm-thick Pt coating. For example, in the profile in Fig 4(d), the Pt coating reduces x-ray transmission from R_{Pt}=-180 μm to -110 μm and from R_{Pt}=120 μm to 165 μm (red and green line pairs represent uncertainty in these values). The 50-70 micron radial extent of this transition is most likely due to motional blurring of the Pt layer, which is moving at the implosion velocity of ~70 μm/ns during the ~1 ns radiographic exposure. Thus the outermost influence of the Pt limb (at the start of the exposure) and the innermost influence of the Pt limb (at the end of the exposure) can be identified. Averaging over the full 4.0 mm height of the radiograph, if the inner (*outer*) Pt influence is used, radii of 116±15 μm (183±15 μm) are found, giving a liner convergence CR=20±3 (*13±1*). The liner's inner radius, $R_{in}(z,t)$, which averages 116 μm, is observed to exhibit only slight long wavelength variations from 95 μm to 130 μm over a height of 4.0 mm. The symmetry at CR=20 is extremely encouraging for MagLIF target designs, which may require only moderate liner convergence ratios (near 25) to achieve 100 kJ DT-equivalent yields on Z [16]. These demonstrated ETI and MRT mitigation strategies are applicable to a large class of magnetically driven implosion platforms, including those for dynamic material properties studies, radiation source development, and ICF.

[1] Knudson, M. D., D. L. Hanson, J. E. Bailey, C. A. Hall, J. R.Asay, and C. Deeney, , Phys. Rev. B **69**, 144209-144220 (2004).

[2] R. E Reinovsky *et al.*, IEEE Trans. Plasma Sci., **30**, 1764–1776 (2002).

[3] J.E. Bailey et al., Nature, **517**, 56 (2015).

[4] J.E. Bailey et al., Phys. Plasmas, **13**, No. 5, 056301 (2006).

[5] G.A. Rochau et al., Plasma Phys. Control. Fusion, **49**, No. 12B, B591-B600 (2007).

[6] M.E. Cuneo et al., IEEE Trans. Plasma Sci., **40**, No. 12, 3222 (2012).

[7] D.D. Ryutov, M. S. Derzon, and M. K. Matzen, Rev. Mod. Phys. **72**, No. 1, 167-223 (2000).

[8] M.G. Haines, Plasma Phys. Control. Fusion **53**, 093001 (2011).

[9] M.A. Liberman, J.S. De Groot, A. Toor, and R.B. Spielman, *Physics of High-Density Z-Pinch Plasmas* (Springer-Verlag, New York, 1999).

[10] M. K. Matzen, B.W. Atherton, M. E. Cuneo, G. L. Donovan, C. A. Hall, M. Herrmann, M. L. Kiefer, R. J. Leeper, G. T. Leifeste, F.W. Long, G. R. McKee, T. A. Mehlhorn, J. L. Porter, L.X. Schneider, K.W. Struve, W. A. Stygar, and E. A. Weinbrecht, Acta Phys. Pol. A 115, 956 (2009).

[11] D.V. Rose, D. R. Welch, E. A. Madrid, C. L. Miller, R. E. Clark, W. A. Stygar, M. E. Savage, G. A. Rochau, J. E. Bailey, T. J. Nash, M. E. Sceiford, K.W. Struve, P. A. Corcoran, and B. A. Whitney, Phys. Rev. ST Accel. Beams 13, 010402 (2010).

[12] M. R. Martin, R. W. Lemke, R. D. McBride, J. P. Davis, D. H. Dolan, M. D. Knudson, K. R. Cochrane, D. B. Sinars, I. C. Smith, M. Savage, W. A. Stygar, K. Killebrew, D. G. Flicker, and M. C. Herrmann, Phys. Plasmas **19**, 056310 (2012).

[13] M. R. Gomez *et al*. Phys. Rev. Lett. **113**, 155003 (2014).

[14] S. A. Slutz, M. C. Herrmann, R. A. Vesey, A. B. Sefkow, D. B. Sinars, D. C. Rovang, K. J. Peterson, and M. E. Cuneo, Phys. Plasmas 17, 056303 (2010).

[15] S. A. Slutz and R. A. Vesey, Phys. Rev. Lett. 108, 025003 (2012).

[16] A.B.Sefkow, S.A. Slutz, J.M. Koning, M.M. Marinak, K.J. Peterson, D.B. Sinars, and R.A. Vesey, Phys. Plasmas **21**, 072711 (2014).

[17] E. G. Harris, Phys. Fluids 5, 1057 (1962).

[18] Y. Y. Lau, J. C. Zier, I. M. Rittersdorf, M. R. Weis, and R. M.vGilgenbach, Phys. Rev. E 83, 066405 (2011).

[19] D.B. Sinars, *et al*. Phys. Plasmas **18**, 056301 (2011).

[20] R.   D. McBride *et al.*, Phys. Rev. Lett. **109**, 135004 (2012).

[21] R. D. McBride, M. R. Martin, R. W. Lemke, J. B. Greenly, C. A. Jennings, D. C. Rovang, D. B. Sinars, M. E. Cuneo, M. C. Herrmann, S. A. Slutz, C. W. Nakhleh, D. D. Ryutov, J.-P. Davis, D. G. Flicker, B. E. Blue, K. Tomlinson, D. Schroen, R. M. Stamm, G. E. Smith, J. K. Moore, T. J. Rogers, G. K. Robertson, R. J. Kamm, I. C. Smith, M. Savage, W. A. Stygar, G. A. Rochau, M. Jones, M. R. Lopez, J. L. Porter, and M. K. Matzen, Phys. Plasmas **20**, 056309 (2013).

[22] K.J. Peterson, T.J. Awe, E.P. Yu, D.B. Sinars, E.S. Field, M.E. Cuneo, M.C. Herrmann, M. Savage, D. Schroen, K. Tomlinson, and C. Nakhleh, Phys. Rev. Lett. **112**, 135002 (2014)

[23] A.H. Nelson and M.G. Haines, Plasma Physics **11**, 811-837 (1969).

[24] Velikhov, E. P., I. V. Novobrantsev, V. D. Pis'mennyi, A. T. Rakhimov, and A. N. Starostin, 1972, Sov. Phys. Dokl. 17, 772.

[25] M.G. Haines, J. Plasma Phys. 12, No. 1, 1-14 (1974).

[26] K. J. Peterson, D. B. Sinars, E. P. Yu,M. C. Herrmann, M. E. Cuneo, S. A. Slutz, I. C. Smith, B.W. Atherton, M. D. Knudson, and C. Nakhleh, Phys. Plasmas 19, 092701 (2012).

[27] V. Oreshkin, R. Baksht, N. Ratakhin, A. Shishlov, K. Khishchenko, P. Levashov, and I. Beilis, Phys. Plasmas 11, 4771 (2004).

[28] V. Oreshkin, Tech. Phys. Lett. 35, 36 (2009).

[29] V. I. Oreshkin, Phys. Plasmas 15, 092103 (2008).

[30] A. G. Rousskikh, V. I. Oreshkin, S. A. Chaikovsky, N. A. Labetskaya, A. V. Shishlov, I. I. Beilis, and R. B. Baksht, Phys. Plasmas 15, 102706 (2008).

[31] K. J. Peterson, E. P. Yu, D. B. Sinars, M. E. Cuneo, S. A. Slutz, J. M. Koning, M. M. Marinak, C. Nakhleh, and M. C. Herrmann, Phys. Plasmas 20, 056305 (2013).

[32] T.J. Awe, R. D. McBride, C. A. Jennings, D. C. Lamppa, M. R. Martin, D. C. Rovang, S. A. Slutz, M. E. Cuneo, A. C. Owen, D. B. Sinars, K. Tomlinson, M. R. Gomez, S. B. Hansen, M. C. Herrmann, J. L. McKenney, C. Nakhleh, G. K. Robertson, G. A. Rochau, M. E. Savage, D. G. Schroen, and W. A. Stygar, Phys. Rev. Lett. **111**, 235005 (2013)

[33] T. J. Awe, C. A. Jennings, R. D. McBride, M. E. Cuneo, D. C. Lamppa, M. R. Martin, D. C. Rovang, D. B. Sinars, S. A. Slutz, A. C. Owen, K. Tomlinson, M. R. Gomez, S. B. Hansen, M. C. Herrmann, M. C. Jones, J. L. McKenney, G. K. Robertson, G. A. Rochau, M. E. Savage, D. G. Schroen, and W. A. Stygar, Phys. Plasmas **21**, 056303 (2014).

[34] G. R. Bennett, I. C. Smith, J. E. Shores, D. B. Sinars, G. Robertson, B.W. Atherton, M. C. Jones, and J. L. Porter, Rev. Sci. Instrum. 79, 10E914 (2008).

[35] H. Tennekes and J.L. Lumley, *A First Course in Turbulence* (MIT Press, Cambridge, MA, 1972).

[36] N.R. Pereira, N. Rostoker, and J.S. Pearlman, J. Appl. Phys. **55**, 704 (1984).

[37] D.C. Rovang *et al.*, Rev. Sci. Instrum. **85**, 124701 (2014).